Exp. Eye Res. (2002) **75**, 347–358
doi:10.1006/exer.2002.2010, available online at http://www.idealibrary.com on IDEAL®

A New View of the Human Trabecular Meshwork Using Quick-freeze, Deep-etch Electron Microscopy

HAIYAN GONG*, JEFFREY RUBERTI, DARRYL OVERBY, MARK JOHNSON AND THOMAS F. FREDDO

[a]*Boston University School of Medicine, Boston, MA 02118, U.S.A.,* [b]*MIT, Cambridge, MA, U.S.A. and* [c]*Northwestern University, Evanston, IL, U.S.A.*

(*Received 17 December 2001 and accepted in revised form 22 February 2002*)

Conventional transmission electron microscopic (TEM) images of the juxtacanalicular tissue (JCT) region of the trabecular meshwork (TM) show flow passages that are much too large to generate significant outflow resistance. The goal of the current study was to use quick-freeze/deep-etch (QF/DE), a technique that better preserves extracellular matrices, to determine if extracellular matrix material fills all the apparently 'open-spaces' that were observed using conventional TEM.

Normal adult human eyes were fixed by immersion or under flow at pressures of 15 or 45 mmHg. The TM and the inner wall of Schlemm's canal (SC) were examined using QF/DE and compared to the observations using conventional TEM.

The structure of the TM, as seen using QF/DE, showed much greater three dimensional ultrastructural detail than was seen with conventional TEM. Open space was confirmed to be present between the trabecular beams. Although significantly more extracellular matrix was observed in the JCT region using QF/DE than by conventional TEM, some micron-sized open-spaces were still present immediately beneath the inner wall of SC. Consistent with prior reports, the basement membrane of the cells lining the inner wall of SC exhibited discontinuities but the basement membrane as seen by QF/DE was much more elaborate and complex than was evident in conventional TEM of immersion-fixed eyes. This basal lamina became less continuous with increasing perfusion pressure.

QF/DE, although difficult and very labor-intensive when used to examine the TM, offers several clear advantages over conventional methods of tissue preparation for ultrastructural study. Although a more complex and less open extracellular matrix structure was seen in the JCT using QF/DE compared with conventional TEM, some open-spaces, similar in size to those seen by TEM, were still observed in this region. The continued presence of such open-spaces in QF/DE images suggests that either the JCT may not generate a significant fraction of outflow resistance in normal eyes or even QF/DE is not sensitive enough to preserve and identify all the extracellular matrix in the JCT region of the TM.

SC appears to exhibit a discontinuous basal lamina like lymphatic channels but, like venules, exhibits a wide lumen and continuous endothelium. Because of these features, and the presence of continuous tight junctions that typify continuous capillaries, but neither lymphatic channels nor venules, SC has traditionally been described as a vessel sui generis. Our observations of perfusion-induced changes in the basal lamina of the inner wall of SC suggest that the discontinuous basal lamina underlying the inner wall of SC may not represent the normal expression of the vessel but may simply be a consequence of the way in which giant vacuoles and their pores give rise to outflow.

Key words: trabecular meshwork; quick-freezing; deep-etching; basement membrane; electron microscopy.

1. Introduction

Mäepea and Bill (1989, 1992) provided experimental evidence to show that outflow resistance in the normal eye is generated within 7–14 μm of the inner wall of Schlemm's canal (SC), presumably within the juxtacanalicular connective tissue (JCT). Previous morphometric studies have shown that flow passages in the JCT, as visualized using conventional transmission election microscopy (TEM), were much too large to generate a significant fraction of outflow resistance (Ethier et al., 1986). This observation has been confirmed by a number of groups (Seiler and Wollensak, 1985; Murphy et al., 1992; Ten Hulzen and Johnson, 1996).

One possible explanation of this apparent discrepancy is the loss of certain extracellular matrix moieties from the JCT region during the processing steps necessary for conventional electron microscopy. This is likely due to (i) collapse of glycosaminoglycans (GAGs) and the concomitant loss of the fine structures of the extracellular matrix (Hascall and Hascall, 1982) and (ii) the actual loss of the extracellular materials themselves (Overby et al., 2001). Quick-freeze/deep-etch (QF/DE) (Heuser and Salpeter, 1979; Heuser and Kirschner, 1980; Heuser, 1989) is a morphologic technique that preserves the extracellular matrix

* Address correspondence to: Haiyan Gong, Department of Ophthalmology, Boston University School of Medicine, 715 Albany Street, Room L-912, Boston, MA 02118, U.S.A. E-mail: hgong@bu.edu

0014-4835/02/$35.00/0

ultrastructure in exquisite detail and allows for visualization of structures not seen using conventional TEM techniques (Kubosawa and Kondo, 1994; Hirsch et al., 1999; Overby et al., 2001). The goal of this study was to use this technique to determine if ultrastructural details were evident in the apparently 'open-spaces' of the JCT, that were not evident using conventional TEM.

2. Materials and Methods

Human Eyes

A total of 10 eye-bank eyes from donors with no known history of eye disease (age 56–89 years) were obtained from National Disease Research Interchange (Philadelphia, PA, U.S.A.), within 24 hr post-mortem. Donor eyes were used in accordance with the guidelines regarding use of human subjects and tissues as outlined in the Helsinki Declaration. Each eye was confirmed to be grossly normal by examination under a dissecting microscope. Four eyes were immersion-fixed (0 mmHg) with 2 % paraformaldehyde, 2·5 % glutaraldehyde in phosphate buffer, (pH 7·3) for 3 hr at room temperature. The remaining eyes were prepared as described below.

Perfusion Procedure

Three pairs of eyes were perfusion-fixed. One eye of each pair was perfusion-fixed at a constant pressure of 15 mmHg. The other eye was perfusion-fixed at 45 mmHg.

Each eye to be perfused was placed in a beaker, covered with saline, and then the beaker was placed into a water bath (34°C). A 25-gauge perfusion needle was inserted through the cornea, placing the tip into the posterior chamber of the eye to prevent anterior chamber deepening. A second 25-gauge needle was then inserted through the cornea with the tip placed into the anterior chamber to serve as the exchange needle. The line leading from the exchange needle was initially clamped off.

A baseline outflow facility was measured at 15 or 45 mmHg. The perfusion fluid used to obtain a baseline facility was Dulbecco's phosphate buffered saline (Life Technologies, Grand Island, NY, U.S.A.) with 5·5 mM glucose added (DBG), pre-filtered through a 0·2 mm cellulose acetate filter (Costar Scientific Corp., Cambridge, MA, U.S.A.). Flow into the eye was controlled using a computer-controlled syringe pump (Model 22, Harvard Apparatus, South Natick, MA, U.S.A.). Pressure signals were digitized using a MacADIOS-8ain A/D converter (GW Instruments, Inc., Somerville, MA, U.S.A.). The control algorithm is described in detail by Whale et al. (1996). Outflow facility was calculated as the ratio of the steady-state flow rate (usually reached in 30 min) to intraocular pressure.

Following measurement of the baseline facility, the eyes were then exchanged with fixative (2 % paraformaldehyde, 2·5 % glutaraldehyde in phosphate buffer, pH 7·3) and then fixed at the perfusion pressure. This was performed by placing the fixative-containing reservoir at a height of 2 cm H_2O above the fixation pressure, and placing the waste reservoir at a height 2 cm H_2O below the fixation pressure. This protocol ensured that the average pressure in the eye was never more than 2 cm H_2O away from the fixation pressure. Both reservoir lines were then opened to allow rapid exchange of the anterior chamber. Approximately 2 ml of fluid was exchanged to flush thoroughly the anterior chamber as well as the fluid lines. A small amount of fluorescein sodium salt (Sigma Chemical Co., St. Louis, MO, U.S.A.) (approximately 10 mg/100 ml of fixative) was added to help visualize the fixative and ensure that the anterior chamber was well exchanged. After the AC exchange, the eyes were perfused from the syringe pumps at the fixation pressure, and outflow facility was again measured.

After either immersion or perfusion fixation, the eyes were opened at the equator. The lens was gently removed and the anterior segment of each eye was cut radially into small wedges. The tissue wedges from each eye were embedded in 7 % agar and 190-μm chopper sections were cut with a Smith-Farquar tissue chopper (DuPont Co., Wilmington, DE, U.S.A.).

Conventional Electron Microscopic Procedure

Some chopper sections were post-fixed for 2 hr at 4°C in 1 % osmium tetroxide and 1·5 % potassium ferrocyanide in distilled water, dehydrated, and embedded in an Epon–Araldite mixture. Thin sections were cut and stained with uranyl acetate and lead citrate. Micrographs were taken on a Philips-300 TEM (Philips, Eindhoven, The Netherlands). At least six to eight sections from more than two blocks per eye were examined.

Quick-freeze/Deep-etch Procedure

Other chopper sections from each specimen were trimmed to contain only trabecular meshwork (TM), SC and a narrow strip of sclera. A few minutes before freezing, each sample was placed into distilled water to remove salts and soluble components that would otherwise precipitate during etching, potentially limiting the depth of etching and obscuring parts of the replica (Heuser and Salpeter, 1979). Tissue samples were placed on a small pad (approximately 5 × 5 mm) of 1 % agar that was placed upon an aluminum slam-tab (Med Vac Inc., St. Louis, MO, U.S.A.) and surrounded by a plastic ring (Med Vac, Inc., St. Louis, MO, U.S.A.) to support the tissue against collapse during impact. The tissue was frozen by rapid contact with an ultrapure copper

block that was cooled to −220°C by an impinging jet of liquid helium. Frozen samples (slam-tab, agar and tissue) were quickly removed and stored under liquid nitrogen. The specimens were mounted onto a copper sled and transferred to a Cressington CFE-60 (Cressington Scientific Instruments, Inc., Watford, U.K.) vacuum chamber (−180°C) held at $<2 \times 10^{-6}$ mbar. The specimens were fractured at −150°C using a new microtome blade (Cressington Scientific Instruments, Inc., Watford, U.K.), taking care to stay within the superficial layer of vitrified ice. To expose the tissue ultrastructure, the specimen holder was warmed to −100°C and the fractured surfaces were etched for 30 min by placing the colder (−180°C) microtome above the specimens. Following etching (sublimation of vitrified water from the specimen onto the colder knife), the specimen holder was allowed to cool while the microtome was held over the specimens to prevent contamination from residual gasses in the vacuum chamber. Once the temperature reached −150°C, the microtome was moved, and the specimens were immediately rotary shadowed at 20° with a mixture of evaporated platinum–carbon. The estimated coating thickness using this method was approximately 1·5 to 2·0 nm as determined by a quartz crystal thin film monitor. Replicas were strengthened by deposition of an additional layer of carbon at an angle of 90°. The specimens were stored in methanol overnight. The tissue was digested in 5% sodium hypochlorite containing 10–15% potassium hydroxide, and remaining replicas were then washed several times in distilled water and floated onto copper grids (Electron Microscopy Sciences, Ft. Washington, PA, U.S.A.).

The procedure for a single immersion-fixed specimen differed from the above. To facilitate the identification of SC, the lumen of the canal was carefully filled with homologous iris pigment in some sections at the beginning of this study. These sections were mounted onto 3 mm gold specimen carriers with a thin layer of 25% polyvinyl alcohol (Gelvatol 20–30; Monsanto, Springfield, MA, U.S.A.) in 25% glycerol. The tissue was plunge-frozen by dropping the specimens and carrier together into liquid propane (−180 to −190°C) using a BAL-TEC TFD 010 plunge-freeze and transfer device (BAL-TEC Limited, Principality of Liechtenstein). The frozen specimens were stored in liquid nitrogen until they were transferred onto a cold copper sled (−150°C) and placed into a Balzers freeze-fracture chamber (BAF-301; Balzers High Vacuum, Santa Ana, CA, U.S.A.) held at $<10^{-6}$ mbar. Fracturing, etching and creation of the replica then proceeded as described above. All replicas were examined and micrographs taken using a Philips-300 TEM (Philips, Eindhoven, The Netherlands).

3. Results

Trabecular Beams

The general ultrastructural architecture of the trabecular beams as seen using the QF/DE method conforms to that seen previously using conventional TEM (Fig. 1(A) and (B)). Although much greater structural detail was seen in the QF/DE images compared with conventional TEM, intertrabecular spaces between adjacent beams were devoid of any detectable matrix using both methods (Fig. 1(A) and (B)). The cytoskeleton of the trabecular endothelial cells (TEC) and their associated organelles were readily seen in the QF/DE specimens (Fig. 1(B)).

By conventional TEM, the basal lamina underlying the TEC consisted of two layers: a thin, electron-lucent lamina rara immediately beneath the TEC that was devoid of structure, and an electron-dense lamina densa of variable thickness, composed of granular and fibrillar material (Fig. 1(A)). Viewed by QF/DE, far more detail was evident in both portions of the basal lamina, revealing a more complex ultrastructure. The lamina rara was clearly thicker in the QF/DE images suggesting that less shrinkage had occurred during processing (Fig. 1(B)). The lamina rara, devoid of structure by conventional TEM (Fig. 1(A)), was seen to be traversed by numerous fibrils (approximately 10 nm in width, 100 nm in length) in QF/DE images (Fig. 1(B)). These fibrils ran perpendicular to the TEC membrane and connected the cells to the more complex matrix of the subadjacent lamina densa. The lamina densa was 170–215 nm thick and had a polygonal meshwork structure (Fig. 1(B)). In conventional TEM, there was little discernable connection between the lamina densa and the underlying connective tissue core of each beam (Fig. 1(A)). But with QF/DE, a rich network of fibers was evident that clearly anchored the basal lamina firmly to the underlying connective tissue core of the beam (Fig. 1(B)).

Viewed by QF/DE, elastic fibers and collagen within the cores of the beams were readily identified based upon their corresponding positions observed using conventional TEM (Fig. 1(A) and (B)). In specimens from older individuals, QF/DE readily distinguished the central microfibrillar component of the elastic fibers from their surrounding sheath material (Fig. 1(B)). A fine cross bridge-like filamentous matrix with a periodicity of 60 nm, that would correspond to the known location of proteoglycans between the collagen fibrils, was observed in the cores of the beams and was especially apparent when the beams were fractured longitudinally. In contrast, these same spaces were essentially devoid of structure in conventional TEM images (Fig. 2(A) and (B)). In some beams, long-spacing collagen was observed, exhibiting the characteristic banding pattern. The apparently solid dark bands seen with conventional TEM consisted of a densely packed fibrillar substructure when viewed by QF/DE (Fig. 3(A) and (B)). No differences were found in

FIG. 1. Micrograph of a cross-section of a trabecular beam from the same 83 year-old normal donor eye, immersion-fixed at 0 mmHg. (A) A conventional TEM view. BL = basal lamina, EL = elastic fiber, SM = sheath material, C = collagen, TEC = trabecular endothelial cell, ITS = Intertrabecular spaces. (B) A QF/DE view reveals that the cytoskeletal architecture of TEC and several cross-fractured mitochondria (arrows) are evident. The basal lamina underlying the TEC consisted of two layers, a lamina rara (LR) and lamina densa (LD). The fibrils spanning the LR connect the TEC membrane with the sub-adjacent matrix of the LD. The EL, their associated SM and the surrounding C are identified based upon their corresponding appearance to the structures observed using conventional TEM (A) (×16 104).

the ultrastructure of the trabecular beams, comparing eyes immersion-fixed at 0 mmHg and those perfusion-fixed at 15 or 45 mmHg, using either method.

JCT and Inner Wall

Initially, we definitively identified the inner wall of SC by the presence of pigment within the adjacent lumen, since it was difficult to control the fracture plane to go through SC and inner wall in every specimen. When we could identify the inner wall and JCT in the replica, the general ultrastructural architecture of this region, as seen using QF/DE, conformed to that using conventional TEM (Fig. 4(A) and (B)). Much greater structural detail and a richer, more complex extra-cellular matrix was visualized in this region by QF/DE

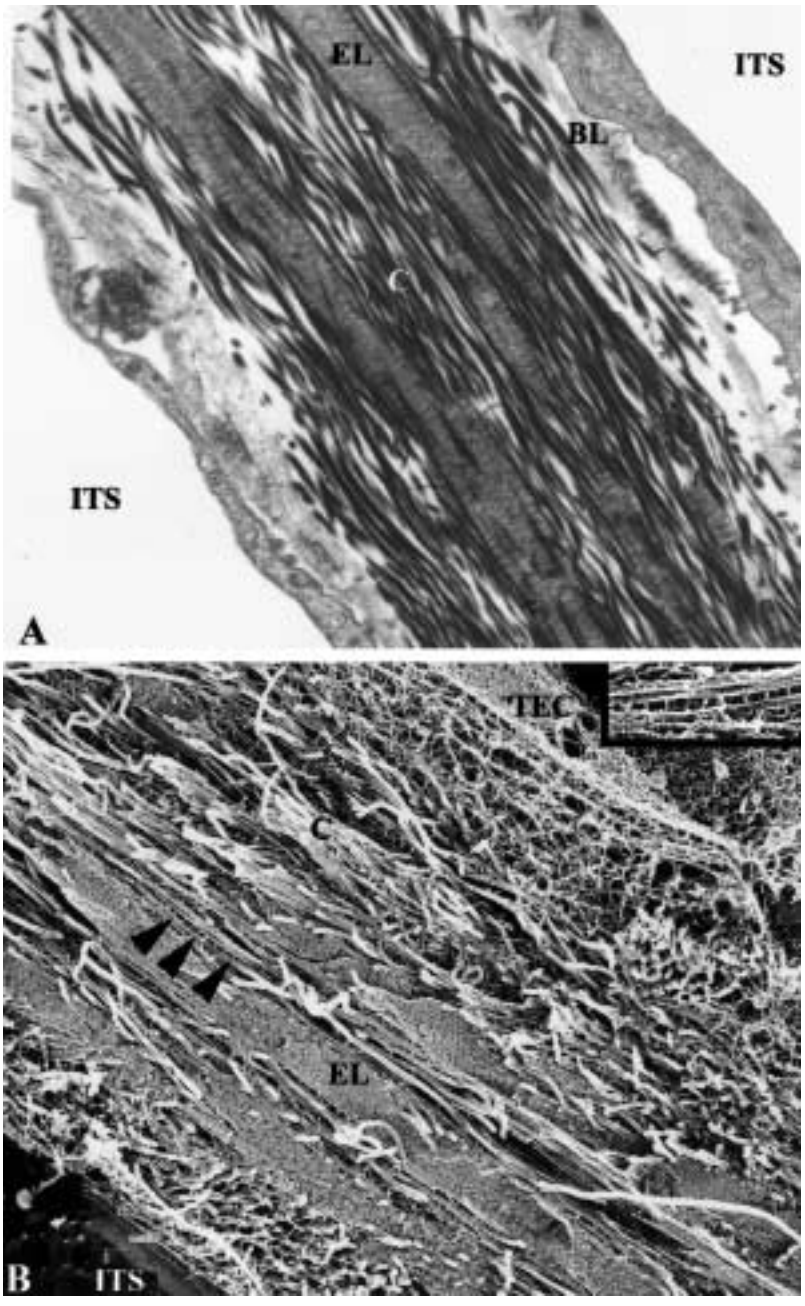

FIG. 2. Conventional (A) and QF/DE (B) micrographs of the core of a trabecular beam from a 75 year-old normal donor eye, immersion-fixed at 0 mmHg. Compared with the structure seen in conventional TEM (A), interfibrillar structures between the collagen fibrils are well visualized by QF/DE (arrowheads) (B), and an enlarged insert of this region. BL = basal lamina, EL = elastic fiber, C = collagen, TEC = Trabecular endothelial cell, ITS = Intertrabecular spaces (×16 380).

than was seen using conventional TEM. Nonetheless, some micron-sized open-spaces still remained evident immediately beneath the inner wall and in the JCT region (Fig. 5(B), 6(B) and 7(B)). Elastic fibers and collagen were identified based upon their corresponding structures observed using conventional TEM (Fig. 4(A) and (B)). A dense network of fibrous elements formed extensive connections between the basal lamina of the inner wall and the elastic fibers that coursed through the JCT region (Fig. 4(B)).

Immersion fixation. In the eyes fixed at 0 mmHg, no giant vacuoles were observed, regardless of the method of preparation. Viewed by conventional TEM (Fig. 4(A)), the discontinuous basal lamina of SC was discernable, but when viewed by QF/DE (Fig. 4(B)), far more detail and complexity was evident. Using QF/DE, this basal lamina looked different from that in the beams, exhibiting a well-defined lamina rara and lamina densa only in certain areas. In these areas, 100–200 nm fibrils, similar to those seen in the trabecular beams were observed spanning the lamina rara, connecting the inner wall cell membrane with the filamentous matrix of the lamina densa. Where present, the thickness of the lamina densa as seen using QF/DE was 400 nm, making it much thicker

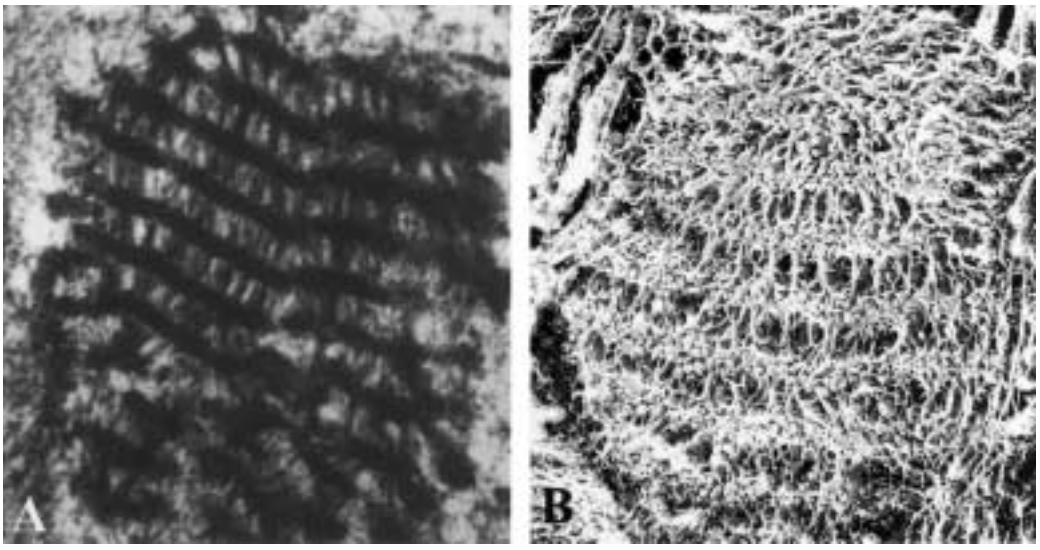

FIG. 3. Micrographs of long-spacing collagen viewed by conventional TEM (A) and QF/DE (B). The characteristic banding pattern is observed by both methods. However, the solid dark bands seen with conventional TEM are revealed to consist of dense fibrillar matrices when viewed by QF/DE method (×66 430).

than that observed using conventional TEM. This 400nm lamina densa observed using QF/DE was subdivided into a fine, almost granular region adjacent to the lamina rara that was 90 nm thick. The remainder of the lamina densa was less compact and merged with the underlying, coarser, extracellular matrix of the JCT region.

Perfusion fixation at 15 mmHg. In the eyes fixed at 15 mmHg, giant vacuoles were observed along the

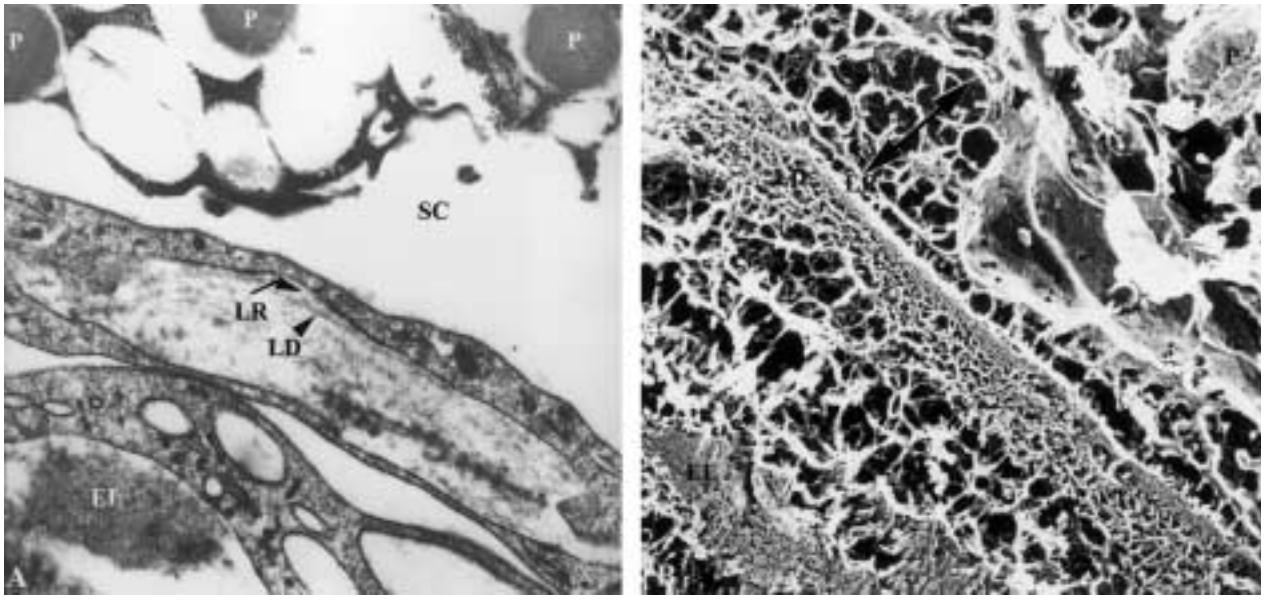

FIG. 4. (A) A conventional TEM micrograph of the inner wall of Schlemm's canal (SC) and JCT region from a 68 year-old normal donor eye, immersion fixed at 0 mmHg. Pigment granules (P) are evident within the canal lumen. The lamina rara (LR) and lamina densa (LD) of the basal lamina are discernable but much greater detail evident in the QF/DE image (B) is not present. Compared to QF/DE image, both layers appear thinner in the conventional TEM, despite being presented at the same magnification, due to greater tissue shrinkage resulting from tissue preparation for TEM. (B) A QF/DE micrograph of inner wall of SC and JCT from the same donor eye immersion-fixed at 0 mmHg. Compared to conventional TEM image, the overall complexity of the extracellular matrix is demonstrably greater. A pigment granule (P) marks the lumen of SC. The inner wall cell and its cytoskeletal architecture can be identified (doubleheaded arrow) by its immediate proximity to the pigment in the lumen of SC. The basal lamina in this region is composed of a LR and a LD. Fibrils of LR clearly extend from the TEC membrane into the underlying matrix of the LD. The LD in the JCT region exhibits a finer, more granular appearance than the LD of cells covering the beams (compare with Fig. 1(A)). Beneath the LD, the filamentous matrix of the JCT demonstrates small open-spaces and finally merging with elastic fibers (EL) (×19 238).

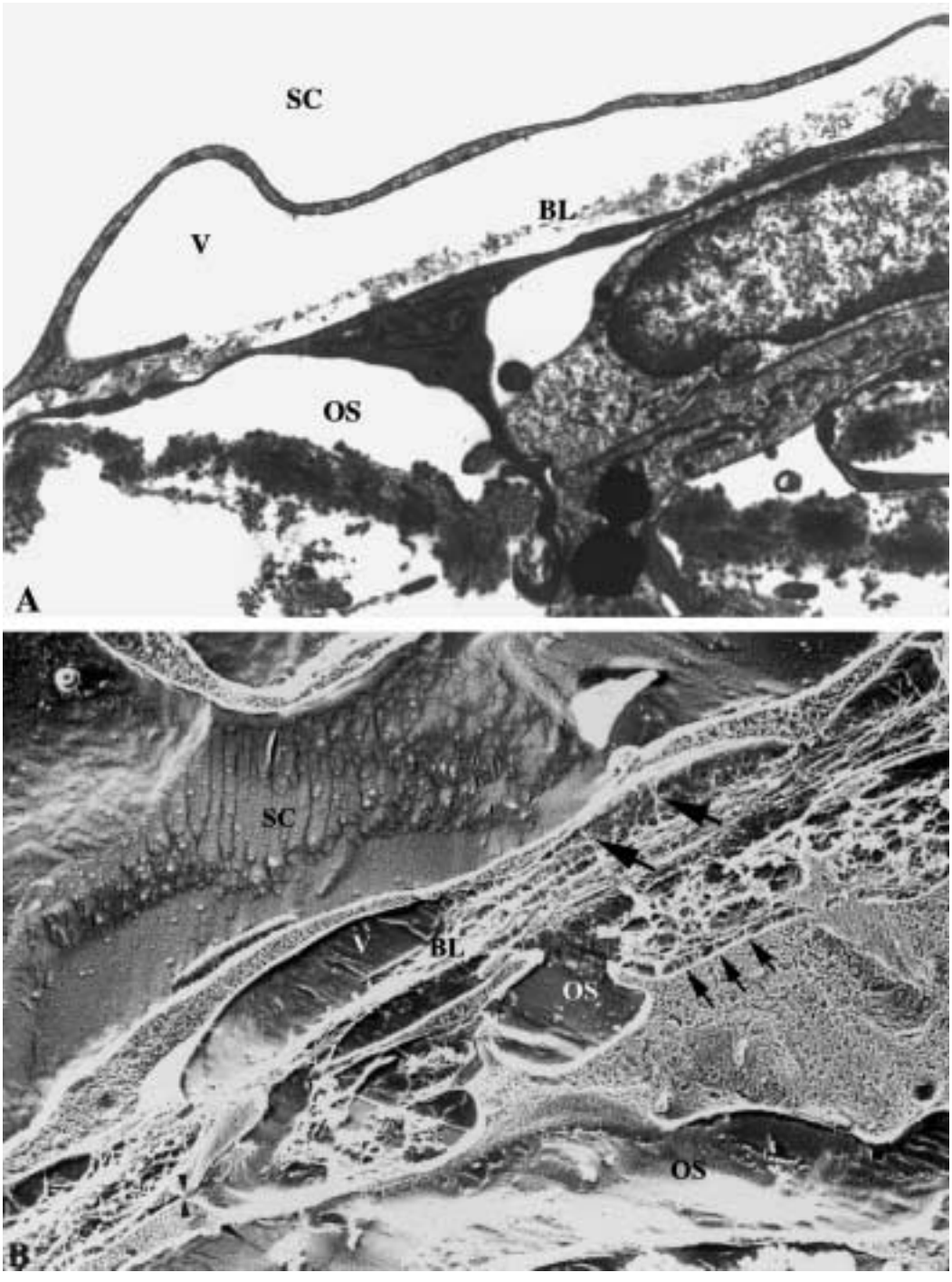

FIG. 5. Micrographs of inner wall of Schlemm's canal (SC) and JCT from an 81 year-old normal donor eye, perfusion-fixed at 15 mmHg IOP. (A) A conventional TEM view shows a vacuolar (V) bullous detachment of the inner wall cell from its basal lamina (BL). The overall complexity of the extracellular matrix in the JCT region is discernably less than seen using QF/DE (B). OS = Open space. (B) A QF/DE view reveals formation of a giant vacuole (V). The V is clearly seen to represent a bullous separation of the cell from its underlying BL. Other cells appear to remain attached via cell-matrix tethers (arrows). A limited amout of OS remains evident in the JCT region. Small arrows show the connection between the JCT cell and the extracellular matrix. Arrowheads show the connections between neighboring JCT cells (×14 563).

inner wall of SC in QF/DE and conventional TEM images (Fig. 5(A) and (B)). The vacuoles appeared empty in both preparations. In the areas of vacuole formation, where the abluminal opening into the vacuole was visible, the inner wall cells appeared to be separated from their underlying basal lamina. Open-spaces were evident in the JCT region by both conventional TEM and QF/DE but the amount of open-space immediately sub adjacent to the inner wall appeared to be less in QF/DE images.

Viewed by conventional TEM, the basal lamina of the inner wall cells had a more irregular, discontinuous and variegated appearance than did the basal lamina underlying the cells lining the trabecular

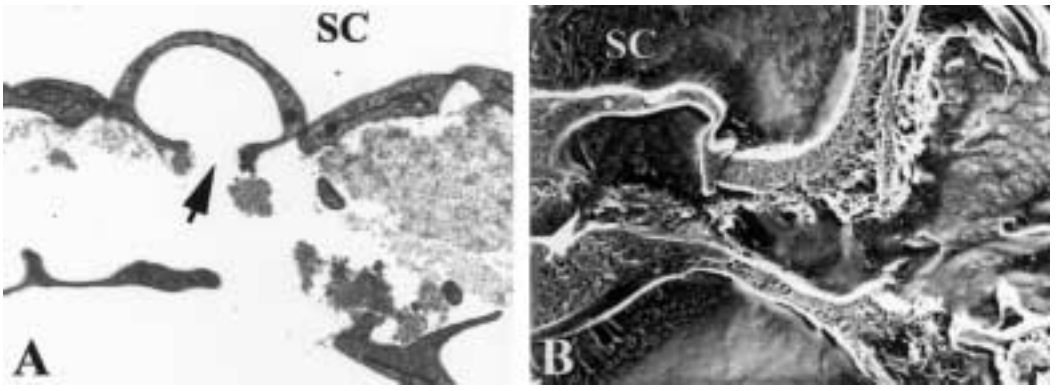

FIG. 6. Micrographs of the inner wall of Schlemm's canal (SC) and JCT from an 81 year-old normal donor eye, perfusion-fixed at 15 mmHg IOP. (A) Conventional TEM view and (B) QF/DE view. Both show vacuoles with discontinuities in their basal laminae (BL) in the area of the contralumenal opening of the vacuole (arrow) (×11 100).

beams. In most areas, a well-delineated lamina rara and lamina densa could not be identified (Fig. 5(A)). When viewed by QF/DE, more details were evident and features suggesting a lamina rara and lamina densa were seen. In locations adjacent to forming giant vacuoles, elongated fibrils were seen tethering the inner wall cells to an underlying dense line suggesting distention of the lamina rara in the early stages of vacuole formation (Fig. 5(B)). In areas where the vacuoles were well-rounded and more fully developed, it was common to observe that the contralumenal opening into the vacuole was no longer bridged by any basal lamina (Fig. 6(A) and (B)). This feature appeared similar in both TEM and QF/DE images but the fibers bridging the lamina rara were evident only with QF/DE.

Perfusion fixation at 45 mmHg. In the eyes perfusion-fixed at 45 mmHg IOP, when viewed by conventional TEM, numerous giant vacuoles were observed along the inner wall of SC. The underlying basal lamina was discontinuous. Compared to the eyes fixed at 0 and 15 mmHg, more breaks were seen along the basal lamina in these eyes (Fig. 7(A)).

When viewed by QF/DE, it was much easier to appreciate the distortion of the inner wall and its underlying matrix produced when large numbers of vacuoles were formed (Fig. 7(B)). No extracellular matrix was observed inside of the giant vacuoles but the amount and complexity of the JCT matrix appeared greater in the QF/DE than in the TEM images (Fig. 7(A) and (B)). Nonetheless, micron-sized open-spaces were seen immediately sub adjacent to the inner wall.

By QF/DE, the basal lamina along the inner wall of SC appeared to be discontinuous. Indeed more areas devoid of underlying basal lamina were observed in these specimens compared with those fixed at 15 mmHg. Compared with eyes fixed at 15 mmHg, similar but longer fibrous tethers were seen connecting the inner wall cells to the JCT matrix (Figs 7(B) and 8(B)). Pores connecting the lumen of giant vacuoles with the lumen of SC were observed using both methods (Fig. 8(A) and (B)).

4. Discussion

QF/DE, although difficult and very labor-intensive when used to examine the TM, offers several clear advantages over conventional methods of tissue preparation for ultrastructural study. Compared with conventional TEM, QF/DE preserves more extracellular matrix and appears to result in less shrinkage than standard protocols that involve chemical extraction, dehydration and embedding in resins.

Previous studies have suggested that 50–75 % of the total aqueous outflow resistance is located between the anterior chamber and the lumen of SC (Grant 1858, 1963; Rosenquist et al., 1989), with most of this resistance residing within 7–14 μm of the inner wall (Mäepea and Bill, 1989, 1992). Previous morphometric studies showed that apparently electron-empty spaces in the JCT, as visualized using conventional TEM, were much too large to generate a significant fraction of outflow resistance, unless these open-spaces were filled with a gel (Ethier et al., 1986). Based upon these studies, we hypothesized that extracellular matrix components within the apparently open-spaces of the JCT that were removed during conventional tissue processing might generate a significant fraction of the outflow resistance in the normal eye. One goal of this study was to use QF/DE to determine if extracellular matrix was present in the apparent 'open-space' of the JCT seen using conventional TEM.

QF/DE did demonstrate a more complex and detailed extracellular matrix. Nonetheless, we continued to observe spaces within the JCT that were apparently devoid of extracellular matrix. The continued presence of open-spaces in the QF/DE casts doubt on the question of whether QF/DE demonstrates sufficient additional matrix to account for a significantly greater fraction of outflow resistance than that calculated from TEM images. An initial comparison of

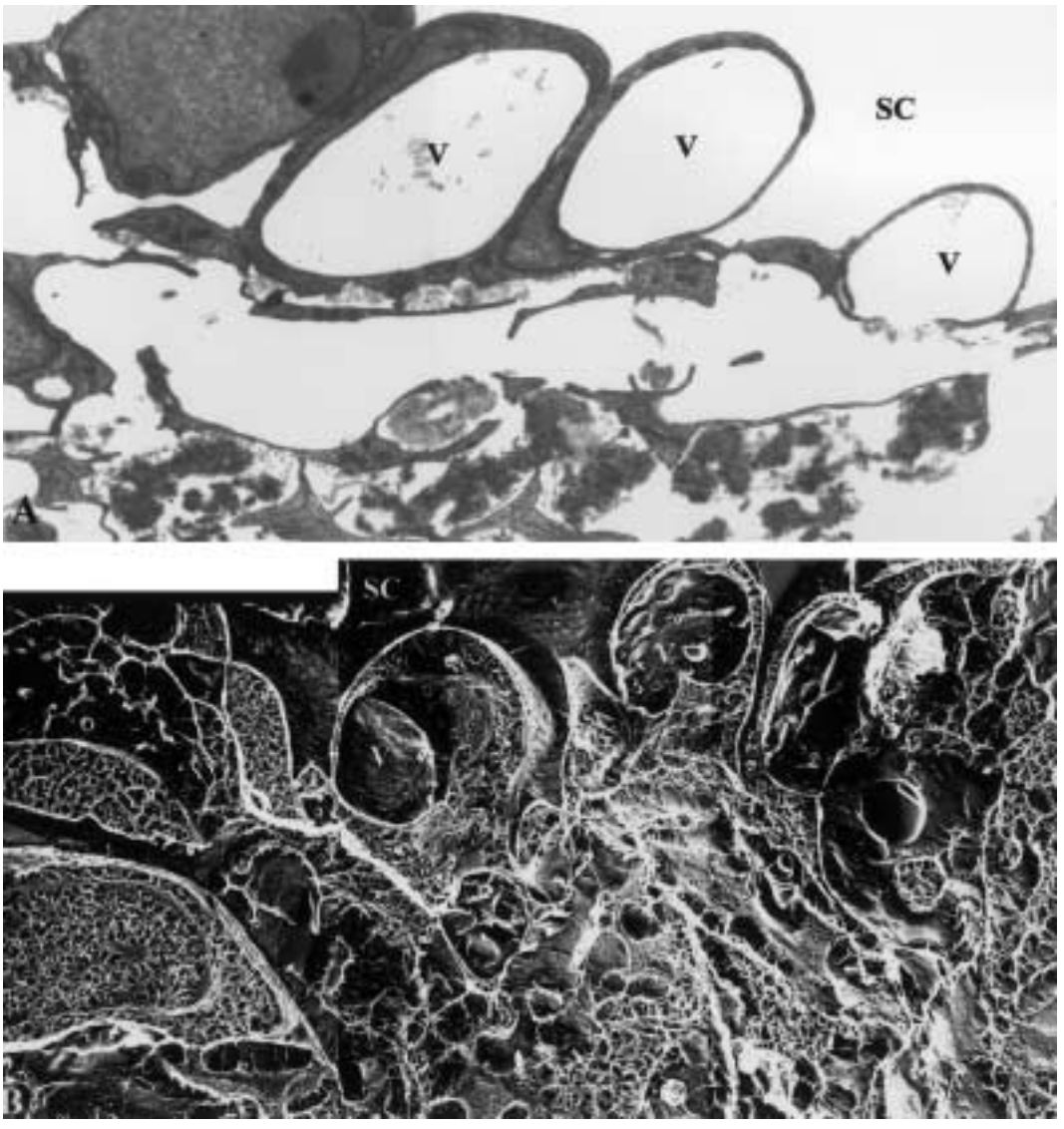

FIG. 7. Conventional TEM (A) and QF/DE micrographs (B) of inner wall of Schlemm's canal (SC) and JCT from an 81 year-old normal donor eye, perfusion-fixed at 45 mmHg IOP. More giant vacuoles (V) are seen along the inner wall of SC than at 15 mmHg, in both TEM and QF/DE images shown at the same magnification. The overall density and complexity of the extracellular matrix remains much greater in the QF/DE image (×6808).

the images obtained by both QF/DE and conventional TEM in this study suggests that the additional matrix visualized by QF/DE might still be insufficient to generate all the resistance in JCT region. It is also possible that even QF/DE is not sensitive enough to preserve and identify all the extracellular matrix in the JCT region of the TM, despite it being a significant improvement over conventional TEM. Still, an examination of the TM of glaucomatous eyes using QF/DE is warranted.

Several components of extracellular matrices, such as GAGs, are known to collapse during the processing steps necessary for conventional TEM (Hascall and Hascall, 1982). In our previous QF/DE study of corneal stroma, we were able to demonstrate a clearly discernable filamentous structure between collagen fibrils using QF/DE, that was not seen using conventional TEM (Overby et al., 2001). In the present study, similar small cross bridge-like filamentous structures were observed between the collagen fibrils by QF/DE, especially in the cores of the trabecular beams. Again these were not seen using conventional TEM. Based on a comparison of the location and distribution of these filamentous structures, with the results of our previous studies using cuprolinic blue to identify sulfated proteoglycans (Gong et al., 1992), the filamentous structures seen by QF/DE are likely to be proteoglycans. It may be that, despite being able to now see the proteoglycans, the GAGs are still collapsed, leaving open-spaces that are not present in vivo. Supporting this view, a previous QF/DE study of vitreous humor, a tissue known to have no open-space in vivo, continued to show open-space using QF/DE (Bos et al., 2001).

As viewed using QF/DE, the basal lamina of the trabecular beams revealed the typical appearance of a

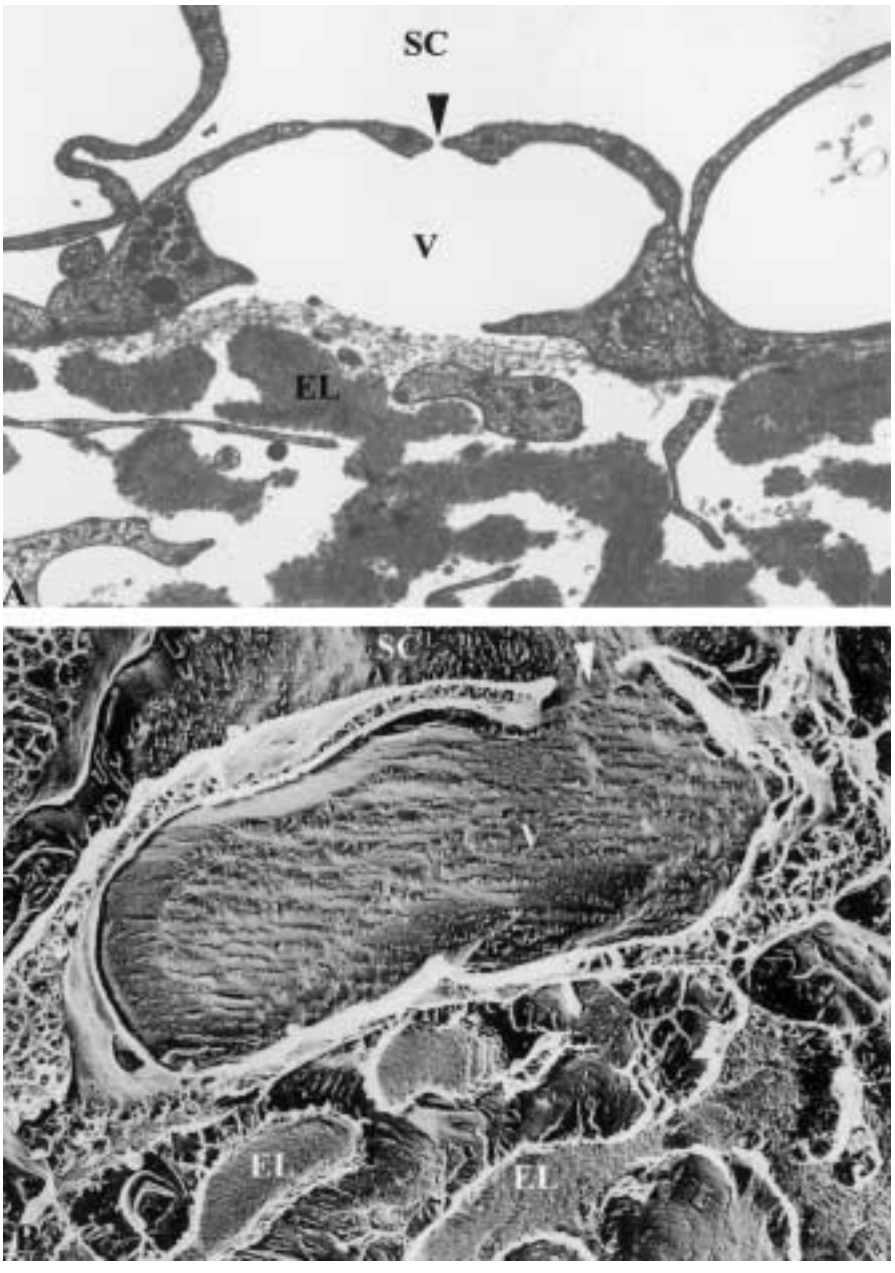

FIG. 8. TEM (A) and QF/DE (B) micrographs of giant vacuoles (V) along the inner wall of Schlemm's canal (SC) in an 81 year-old normal donor eye perfusion-fixed at 45 mmHg IOP. A pore is seen in the wall of each vacuole, opening into the lumen of SC (arrowhead). Elastic fibers = (EL) (×14 040).

lamina rara and lamina densa, similar to previous observations in the glomerular basement membrane (Kubosawa and Kondo, 1985; Takami et al., 1991). The lamina rara, which was observed to be an electron-lucent layer using conventional TEM, was seen to be crossed by numerous fine filaments using QF/DE. Furthermore, the lamina rara was seen to be thicker using QF/DE in comparison to the TEM images, suggesting that shrinkage of the basal lamina architecture had occurred during processing for conventional TEM (Chan and Inoue, 1994).

By contrast, the basal lamina of the endothelial cells lining the inner wall of SC was discontinuous. This is consistent with prior studies using conventional TEM. In their studies, Raviola and Raviola (1981) concluded that the presence of a discontinuous basal lamina around the continuous endothelium of SC qualified it as a vessel sui generis. This conclusion was reached because SC appeared to have a discontinuous basal lamina like a lymphatic channel but had a wide lumen and continuous endothelium like a venule. SC also exhibits continuous tight junctions like those that typify blood capillaries rather than either lymphatics or venules. Observations of perfusion-induced changes in the basal lamina of the inner wall of SC in the present study suggest that the discontinuity of the basal lamina is not the true expression of the endothelium

but is a consequence of the way in which flow traverses its endothelium.

In previous studies by our group, using cuprolinic blue in combination with pre-digestion using specific enzymes, heparan sulfate proteoglycan was demonstrated to be present in the lamina rara of the basal laminae in both the beams and the inner wall of SC (Gong et al., 1992). Heparan sulfate is known to participate in connecting endothelial cells with the lamina densa of their basal lamina (Gong et al., 1992). Combining the results of these previous studies with the present QF/DE, it is reasonable to conclude that heparan sulfate forms at least a portion of the filaments observed by QF/DE that span the lamina rara of the basal lamina in the meshwork. A more detailed examination of possible changes in these filaments with age might be valuable. Heparan sulfate has been shown to decrease with age in the meshwork (Gong et al., 1992). It would be logical to suggest that loss of the filaments spanning the lamina rara, that were identified in the present study using QF/DE, might contribute to the previously documented loss of TEC with age (Alvarado et al., 1981, 1984).

From our current observations, it would appear that the process of giant vacuole formation may begin with dilation of the lamina rara and stretching of the fibers seen to traverse it. Ultimately, separation of the basal surface of the inner wall cell from its basal lamina occurs, with subsequent distention of the cell(s) into the vacuolar configuration. At this stage, the lamina densa, coursing along beneath the bullous distention of the inner wall cell(s) was usually intact. But in vacuoles in which a pore was observed, the entire basal lamina was usually absent underlying the ablumenal opening into the vacuole. This suggests the possibility that the discontinuities in the basal lamina along the inner wall of SC are a secondary consequence of vacuole and pore formation rather than the unique expression of a vessel sui generis as has been previously suggested.

Consistent with this hypothesis, in the present study, we also noticed that as perfusion pressure increased, more discontinuities seemed to be found in the basal lamina of the inner wall. Additional morphometric studies of this phenomenon will be necessary before we can determine whether this loss of basal lamina is merely a secondary consequence of flow or a possible regulatory factor in the process.

Acknowledgements

This work was supported by NIH grant #EY-09699, National Glaucoma Research, a program of the American Health Assistance Foundation and by unrestricted departmental grants from Research to Prevent Blindness, Inc., and The Massachusetts Lions Eye Research Fund, Inc. to the Boston University. The technical assistance of Rozanne Richman, M.S. is most gratefully acknowledged.

References

Alvarado, J., Murphy, C. and Juster, R. (1984). Trabecular meshwork cellularity in primary open-angle glaucoma and nonglaucomatous normals. *Ophthalmology* **91**, 564–79.

Alvarado, J., Murphy, C., Polansky, J. and Juster, R. (1981). Age-related changes in trabecular meshwork cellularity. *Invest. Ophthalmol. Vis. Sci.* **21**, 714–27.

Bos, K. J., Holmes, D. F., Meadows, R. S., Kadler, K. E., McLeod, D. and Bishop, P. N. (2001). Collagen fibril organisation in mammalian vitreous by freeze etch/rotary shadowing electron microscopy. *Micron* **32**, 301–6.

Chan, F. L. and Inoue, S. (1994). Lamina lucida of basement membrane: an artefact. *Microsc. Res. Tech.* **28**, 48–59.

Ethier, C. R., Kamm, R. D., Palaszewski, B. A., Johnson, M. C. and Richardson, T. M. (1986). Calculations of flow resistance in the juxtacanalicular meshwork. *Invest. Ophthalmol. Vis. Sci.* **27**, 1741–50.

Grant, W. M. (1858). Further studies on facility of flow through the trabecular meshwork. *Arch. Ophthalmol.* **60**, 523.

Grant, W. M. (1963). Experimental aqueous perfusion in enucleated human eyes. *Arch. Ophthalmol.* **69**, 783–801.

Gong, H., Freddo, T. F. and Johnson, M. (1992). Age-related changes of sulfated proteoglycans in the normal human trabecular meshwork. *Exp. Eye Res.* **55**, 691–709.

Hascall, V. C. and Hascall, G. K. (1982). Proteoglycans In: *Cell Biology of Extracellular Matrix*. (Hay, E. D., Ed.) pp. 39–63. Plenum: New York, NY, U.S.A.

Heuser, J. (1989). Protocol for 3-D visualization of molecules on mica via the quick-freeze, deep-etch technique. *J. Electron. Microsc. Tech.* **13**, 244–63.

Heuser, J. E. and Kirschner, M. W. (1980). Filament organization revealed in platinum replicas of freeze-dried cytoskeletons. *J. Cell Biol.* **86**, 212–34.

Heuser, J. E. and Salpeter, S. R. (1979). Organization of acetylcholine receptors in quick-frozen, deep-etched, and rotary-replicated Torpedo postsynaptic membrane. *J. Cell Biol.* **82**, 150–73.

Hirsch, M., Noske, W., Prenant, G. and Renard, G. (1999). Fine structure of the developing avian corneal stroma as revealed by quick-freeze/deep-etch electron microscopy. *Exp. Eye Res.* **69**, 267–77.

Kubosawa, H. and Kondo, Y. (1985). Ultrastructural organization of the glomerular basement membrane as revealed by a deep-etch replica method. *Cell Tiss. Res.* **242**, 33–9.

Kubosawa, H. and Kondo, Y. (1994). Quick-freeze, deep-etch studies of renal basement membranes. *Microsc. Res. Tech. 1* **28**, 2–12.

Mäepea, O. and Bill, A. (1989). The pressures in the episcleral veins, Schlemm's canal and the trabecular meshwork in monkeys: effects of changes in intraocular pressure. *Exp. Eye Res.* **49**, 645–63.

Mäepea, O. and Bill, A. (1992). Pressures in the juxtacanalicular tissue and Schlemm's canal in monkeys. *Exp. Eye Res.* **54**, 879–83.

Murphy, C. G., Johnson, M. and Alvarado, J. A. (1992). Juxtacanalicular tissue in pigmentary and primary open angle glaucoma. The hydrodynamic role of pigment and other constituents. *Arch. Ophthalmol.* **110**, 1779–85.

Overby, D., Ruberti, J., Gong, H., Freddo, T. F. and Johnson, M. (2001). Specific hydraulic conductivity of corneal stroma as seen by quick-freeze/deep etch. *J. Biomech. Eng.* **123**, 154–61.

Raviola, G. and Raviola, E. (1981). Paracellular route of aqueous outflow in the trabecular meshwork and canal of Schlemm. A freeze-fracture study of the

endothelial junctions in the sclerocorneal angel of the macaque monkey eye. *Invest. Ophthalmol. Vis. Sci.* **21**, 52–72.

Rosenquist, R., Epstein, D., Melamed, S., Johnson, M. and Grant, W. M. (1989). Outflow resistance of enucleated human eyes at two different perfusion pressures and different extents of trabeculotomy. *Curr. Eye Res.* **8**, 1233–40.

Seiler, T. and Wollensak, J. (1985). The resistance of the trabecular meshwork to aqueous humor outflow. *Graefe's Arch. Clin. Exp. Ophthalmol.* **223**, 88–91.

Takami, H., Naramoto, A., Shigematsu, H. and Ohno, S. (1991). Ultrastructure of glomerular basement membrane by quick-freeze and deep-etch methods. *Kidney Int.* **39**, 659–64.

Ten Hulzen, R. D. and Johnson, D. H. (1996). Effect of fixation pressure on juxtacanalicular tissue and Schlemm's canal. *Invest. Ophthalmol. Vis. Sci.* **37**, 114–24.

Whale, M. D., Grodzinsky, A. J. and Johnson, M. (1996). The effect of aging and pressure on the specific dydraulic conductity of the aortic wall. *Biorheology* **33**, 17–44.